Stellar Pulsation

1 ■ OBSERVATIONS OF PULSATING STARS

In August of 1595, a Lutheran pastor and amateur astronomer named David Fabricius (1564–1617) observed the star *o* Ceti. As he watched over a period of months, the brightness of this second-magnitude star in the constellation Cetus (the Sea Monster) slowly faded. By October, the star had vanished from the sky. Several more months passed as the star eventually recovered and returned to its former brilliance. In honor of this miraculous event, *o* Ceti was named Mira, meaning "wonderful."

Mira continued its rhythmic dimming and brightening, and by 1660 the 11-month period of its cycle was established. The regular changes in brightness were mistakenly attributed to dark "blotches" on the surface of a rotating star. Supposedly, Mira would appear fainter when these dark areas were turned toward Earth.

Figure 1 shows the *light curve* of Mira for a 51-year interval. Today astronomers recognize that the changes in Mira's brightness are due not to dark spots on its surface but to the fact that Mira is a **pulsating star**, a star that dims and brightens as its surface expands and contracts. Mira is the prototype of the **long-period variables**, stars that have somewhat irregular light curves and pulsation periods between 100 and 700 days.

Nearly two centuries elapsed before another pulsating star was discovered. In 1784 John Goodricke (1764–1786) of York, England, found that the brightness of the star δ Cephei varies regularly with a period of 5 days, 8 hours, 48 minutes. This discovery cost Goodricke his life; he contracted pneumonia while observing δ Cephei and died at the age of 21. The light curve of δ Cephei, shown in Fig. 2, is less spectacular than that of *o* Ceti. It varies by less than one magnitude in brightness and never fades from view. Nevertheless, pulsating stars similar to δ Cephei, called **classical Cepheids**, are vitally important to astronomy.

The Period–Luminosity Relation

By 2005, nearly 40,000 pulsating stars had been cataloged by astronomers. One woman, Henrietta Swan Leavitt (1868–1921; see Fig. 3), discovered more than 5% of these stars

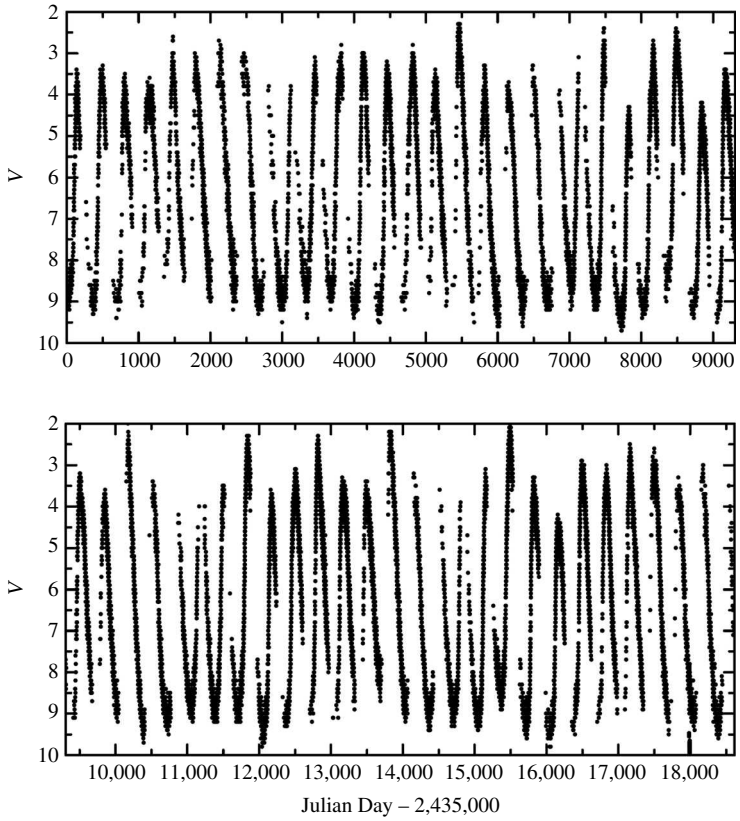

FIGURE 1 The light curve of Mira from September 14, 1954 (JD 2,435,000) through September 2005. Recall that magnitudes dimmer than 6 are undetectable to the unaided eye. (We acknowledge with thanks the variable-star observations from the AAVSO International Database contributed by observers worldwide.)

while working as a "computer" for Edward Charles Pickering (1846–1919) at Harvard University. Her tedious task was to compare two photographs of the same field of stars taken at different times and detect any star that varied in brightness. Eventually she discovered 2400 classical Cepheids with periods between 1 and 50 days, most of them located in the Small Magellanic Cloud (SMC). Leavitt took advantage of this opportunity to investigate the nature of the classical Cepheids in the SMC. Noticing that the more luminous Cepheids took longer to go through their pulsation cycles, she plotted the apparent magnitudes of these SMC stars against their pulsation periods. The resulting graph, shown in Fig. 4, demonstrated that the apparent magnitudes of classical Cepheids are closely correlated with their periods, with an uncertainty of only $\Delta m \approx \pm 0.5$ at a given period.

Because all of the stars in the Small Magellanic Cloud are roughly the same distance from us (about 61 kpc), the differences in their apparent magnitudes must be the same as the differences in their absolute magnitudes. Thus the

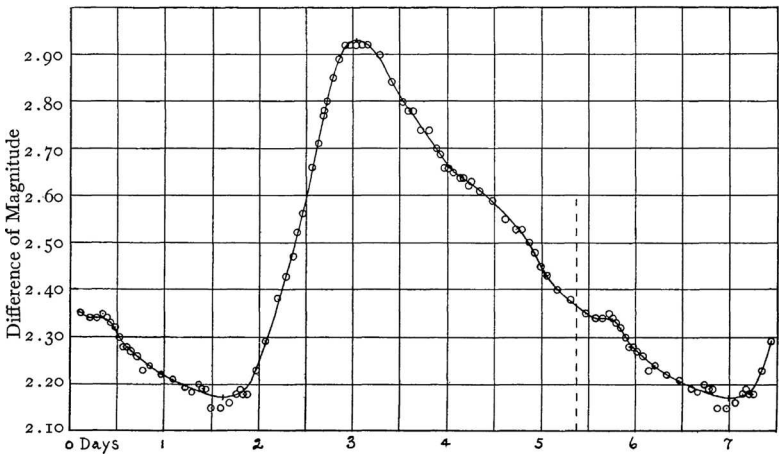

FIGURE 2 The light curve of δ Cephei. Its pulsation period is 5.37 days. (Figure from Stebbins, Joel, *Ap. J.*, *27*, 188, 1908.)

FIGURE 3 Henrietta Swan Leavitt (1868–1921). (Courtesy of Harvard College Observatory.)

observed differences in these stars' apparent brightnesses must reflect intrinsic differences in their luminosities. Astronomers were excited at the prospect of determining the absolute magnitude or luminosity of a distant Cepheid simply by timing its pulsation, because knowing both a star's apparent and absolute magnitudes allows the distance of the star to be easily determined from the distance modulus. This would permit the measurement of large distances in the universe, far beyond the limited range of parallax techniques. The only stumbling block was the calibration of Leavitt's relation. An independent distance to a

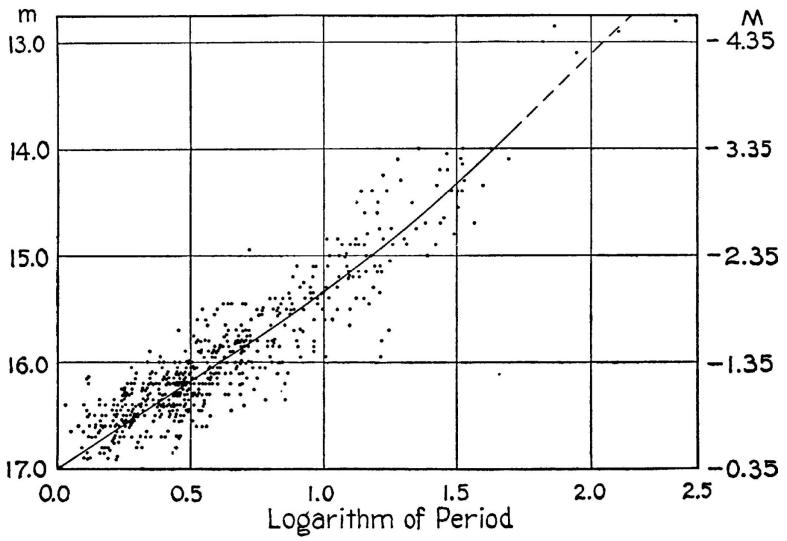

FIGURE 4 Classical Cepheids in the Small Magellanic Cloud, with the period in units of days. (Figure from Shapley, *Galaxies*, Harvard University Press, Cambridge, MA, 1961.)

single Cepheid had to be obtained to measure its absolute magnitude and luminosity. Once this difficult chore was accomplished, the resulting **period–luminosity relation** could be used to measure the distance to any Cepheid.

The nearest classical Cepheid is Polaris, some 200 pc away. In the early twentieth century, this distance was too great to be reliably measured by stellar parallax. However, in 1913, Ejnar Hertzsprung succeeded in using the longer baseline provided by the Sun's motion through space, together with statistical methods, to find the distances to Cepheids having a specified period. (The measurement of the absolute magnitude of a Cepheid is also complicated by the dimming effect of interstellar extinction.)

The calibrated period–luminosity relation depicted in Fig. 5 for the V band is described by

$$\boxed{M_{\langle V\rangle} = -2.81 \log_{10} P_{\rm d} - 1.43,} \tag{1}$$

where $M_{\langle V\rangle}$ is the average absolute V magnitude and $P_{\rm d}$ is the pulsation period in units of days. In terms of the average luminosity of the star, the relation is given by

$$\log_{10} \frac{\langle L\rangle}{L_\odot} = 1.15 \log_{10} P_{\rm d} + 2.47. \tag{2}$$

Astronomers can substantially decrease the scatter in the period–luminosity relation by making observations in infrared wavelengths where interstellar extinction is less of a problem. One such fit, made using magnitudes measured in the infrared H band (centered at 1.654 μm), is illustrated in Fig. 6(a). The data are for 92 Cepheids in the Large

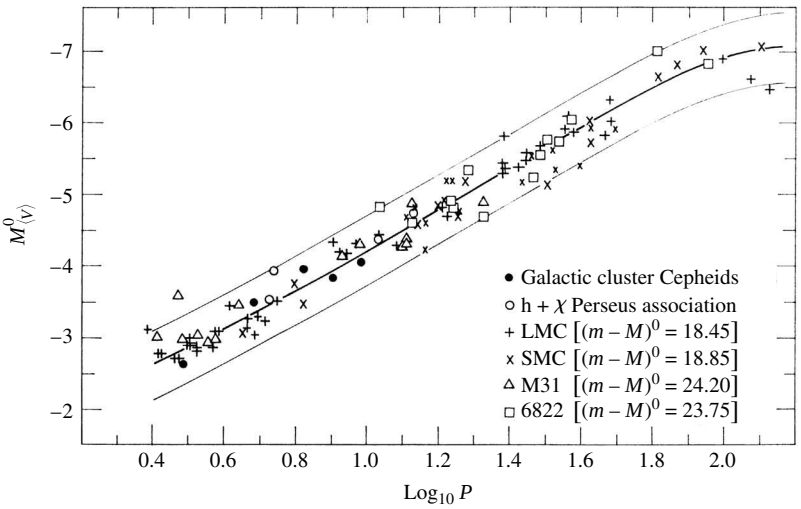

FIGURE 5 The period–luminosity relation for classical Cepheids. (Figure adapted from Sandage and Tammann, *Ap. J.*, *151*, 531, 1968.)

Magellanic Cloud. The infrared period–luminosity fit is given by

$$\boxed{H = -3.234 \log_{10} P_{\mathrm{d}} + 16.079.} \tag{3}$$

The scatter can be further reduced by adding a color term to the fit. Using the infrared color index $J - K_s$, Fig. 6(b) shows that the fit is indeed somewhat tighter (J and K_s are centered at 1.215 μm and 2.157 μm, respectively). The fit for this **period–luminosity–color relation** is given by

$$\boxed{H = -3.428 \log_{10} P_{\mathrm{d}} + 1.54\langle J - K_s\rangle + 15.637.} \tag{4}$$

Classical Cepheids provide astronomy with its third dimension and supply the foundation for the measurement of extragalactic distances. Because Cepheids are supergiant stars (luminosity class Ib), about fifty times the Sun's size and thousands of times more luminous, they can be seen over intergalactic distances. They serve as "standard candles," beacons scattered throughout the night sky that serve as mileposts for astronomical surveys of the universe.

The Pulsation Hypothesis for Brightness Variations

The important use of Cepheids as cosmic distance indicators does not require an understanding of the physical reasons for their light variations. In fact, the observed changes in brightness were once thought to be caused by tidal effects in the atmospheres of binary stars. However, in 1914 the American astronomer Harlow Shapley (1885–1972) argued that the binary theory was fatally flawed because the size of the star would exceed the size of the

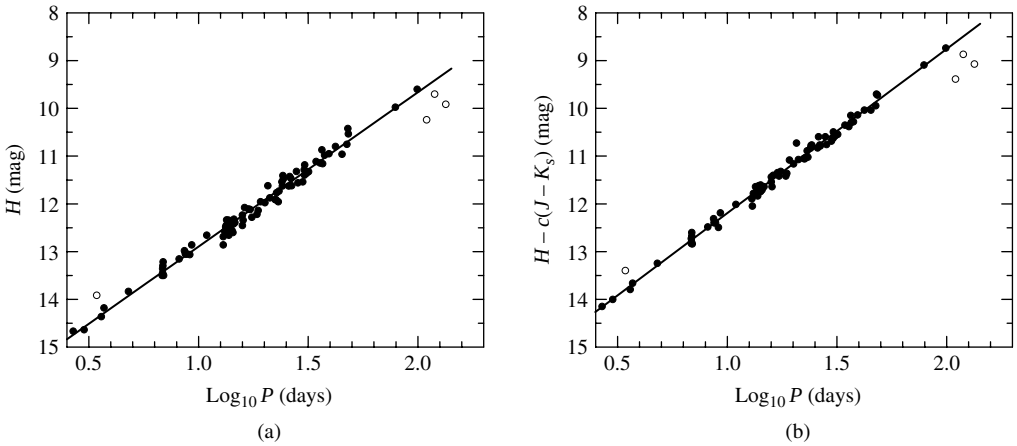

FIGURE 6 (a) The infrared period–luminosity relation for 92 Cepheids in the Large Magellanic Cloud. The infrared H band was used for the observations. The open circles represent four Cepheids that were excluded from the least-squares linear fit. (b) The period–luminosity–color relation for the same Cepheids. (Data from Persson, S. E., et al., *Astron. J.*, *128*, 2239, 2004.)

orbit for some variables. Shapley advanced an alternative idea: that the observed variations in the brightness and temperature of classical Cepheids were caused by the radial pulsation of single stars. He proposed that these stars were rhythmically "breathing" in and out, becoming alternately brighter and dimmer in the process. Four years later Sir Arthur Stanley Eddington provided a firm theoretical framework for the pulsation hypothesis, which received strong support from the observed correlations among the variations in brightness, temperature, and surface velocity throughout the pulsation cycle. Figure 7 shows the measured changes in magnitude, temperature, radius, and surface velocity for δ Cephei. The change in brightness is primarily due to the roughly 1000 K variation in δ Cephei's surface temperature; the accompanying change in size makes a lesser contribution to the luminosity. Although the total excursion of δ Cephei's surface from its equilibrium radius is large in absolute terms (a bit more than the diameter of the Sun), it is still only about 5% to 10% of the size of this supergiant star. The spectral type of δ Cephei changes continuously throughout the cycle, varying between F5 (hottest) and G2 (coolest). A careful examination of Fig. 7 reveals that the magnitude and surface velocity curves are nearly identical in shape. Thus, the star is brightest when its surface is expanding outward most rapidly, *after* it has passed through its minimum radius. Later in this chapter we will see that the explanation of this **phase lag** of maximum luminosity behind minimum radius has its origin in the mechanism that maintains the oscillations.

The Instability Strip

The Milky Way Galaxy is estimated to contain several million pulsating stars. Considering that our Galaxy consists of several hundred billion stars, this implies that stellar pulsation must be a transient phenomenon. The positions of the pulsating variables on the H–R diagram (see Fig. 8) confirm this conclusion. Rather than being located on the main sequence, where stars spend most of their lives, the majority of pulsating stars occupy

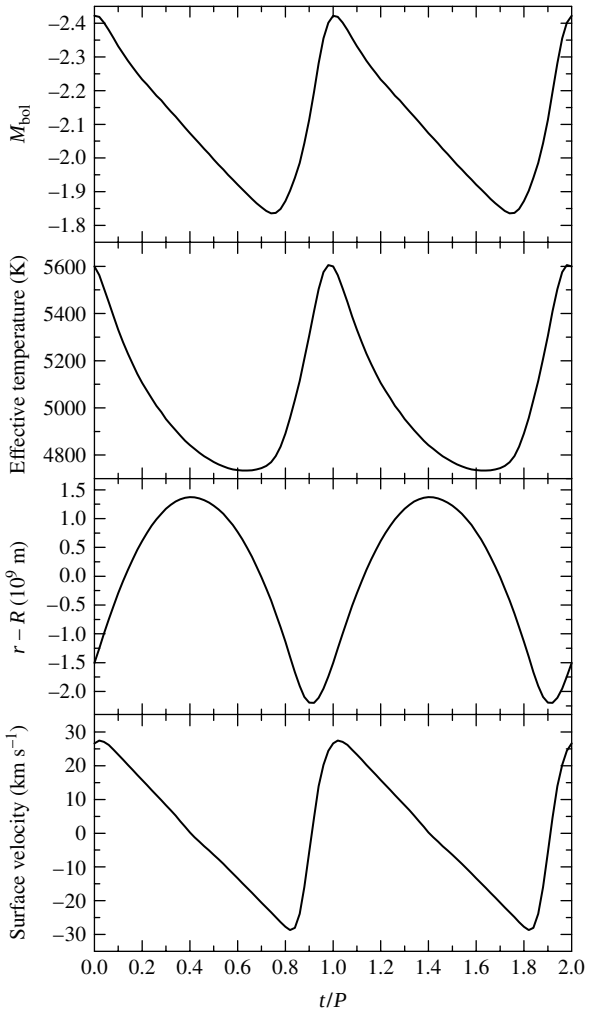

FIGURE 7 Observed pulsation properties of δ Cephei, a typical classical Cepheid. (Data from Schwarzschild, *Harvard College Observatory Circular*, *431*, 1938.)

a narrow (about 600–1100 K wide), nearly vertical **instability strip** on the right-hand side of the H–R diagram. Theoretical evolutionary tracks for stars of various masses are also shown in Fig. 8. As stars evolve along these tracks, they begin to pulsate as they enter the instability strip and cease their oscillations upon leaving. Of course, evolutionary timescales are far too long for us to observe the onset and cessation of a single star's oscillations, but several stars have been caught in the final phase of their pulsational history.

Some Classes of Pulsating Stars

Astronomers have divided pulsating stars into several classes. Some of these are listed in Table 1. The W Virginis stars are metal-deficient (Population II) Cepheids and are

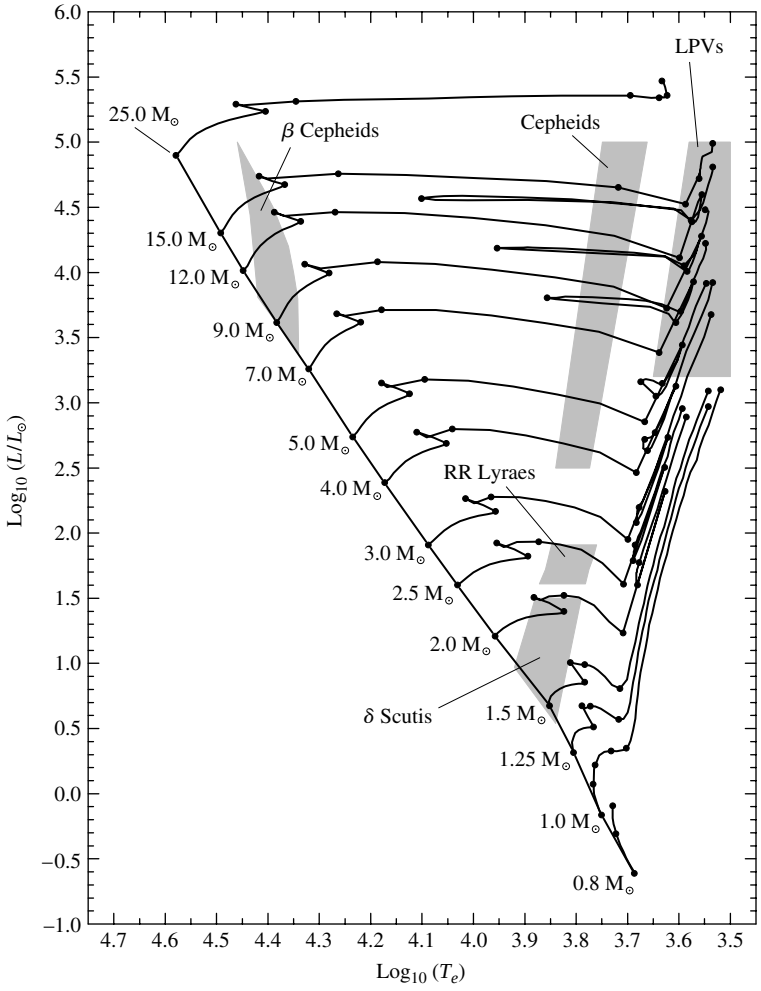

FIGURE 8 Pulsating stars on the H–R diagram. (Data for the evolutionary tracks from Schaller, et al., *Astron. Astrophys. Suppl.*, *96*, 269, 1992.)

about four times less luminous than classical Cepheids with the same period. Their period–luminosity relation is thus lower than and parallel to the one shown for the classical Cepheids in Fig. 5. RR Lyrae stars, also Population II, are horizontal-branch stars found in globular clusters. Because all RR Lyrae stars have nearly the same luminosity, they are also useful yardsticks for distance measurements. The δ Scuti variables are evolved F stars found near the main sequence of the H–R diagram. They exhibit both radial and nonradial oscillations; the latter is a more complicated motion that will be discussed in Section 4. Below the main sequence (not shown in Fig. 8) are the pulsating white dwarfs, called ZZ Ceti stars.

All of the types of stars listed thus far lie within the instability strip, and they share a common mechanism that drives the oscillations. The long-period variables such as Mira

TABLE 1 Pulsating Stars. (Adopted from Cox, *The Theory of Stellar Pulsation*, Princeton University Press, Princeton, NJ, 1980.)

Type	Range of Periods	Population Type	Radial or Nonradial
Long-Period Variables	100–700 days	I,II	R
Classical Cepheids	1–50 days	I	R
W Virginis stars	2–45 days	II	R
RR Lyrae stars	1.5–24 hours	II	R
δ Scuti stars	1–3 hours	I	R,NR
β Cephei stars	3–7 hours	I	R,NR
ZZ Ceti stars	100–1000 seconds	I	NR

and the β Cephei stars are located outside of the instability strip occupied by the classical Cepheids and RR Lyrae stars. Their unusual positions on the H–R diagram will be discussed in the next section.

2 ■ THE PHYSICS OF STELLAR PULSATION

Geologists and geophysicists have obtained a wealth of information about Earth's interior from their study of the seismic waves produced by earthquakes and other sources. In the same manner, astrophysicists model the pulsational properties of stars to understand better their internal structure. By numerically calculating an evolutionary sequence of stellar models and then comparing the pulsational characteristics (periods, amplitudes, and details of the light and radial velocity curves) of the models with those actually observed, astronomers can further test their theories of stellar structure and evolution and obtain a detailed view of the interior of a star.

The Period–Density Relation

The radial oscillations of a pulsating star are the result of sound waves resonating in the star's interior. A rough estimate of the pulsation period,[1] Π, may be easily obtained by considering how long it would take a sound wave to cross the diameter of a model star of radius R and constant density ρ. The adiabatic sound speed is given by,

$$v_s = \sqrt{\frac{\gamma P}{\rho}}.$$

The pressure may be found for hydrostatic equilibrium, using the (unrealistic) assumption of constant density. Thus

[1]Throughout the following discussion, Π will be used to designate the pulsation period so that it is not confused with the pressure, P. Π is commonly used for the pulsation period in stellar pulsation theory studies. (T, another symbol commonly used for period, would lead to confusion with temperature.)

$$\frac{dP}{dr} = -\frac{GM_r\rho}{r^2} = -\frac{G\left(\frac{4}{3}\pi r^3\rho\right)\rho}{r^2} = -\frac{4}{3}\pi G\rho^2 r.$$

This is readily integrated using the boundary condition that $P = 0$ at the surface to obtain the pressure as a function of r,

$$P(r) = \frac{2}{3}\pi G\rho^2\left(R^2 - r^2\right). \tag{5}$$

Thus the pulsation period is roughly

$$\Pi \approx 2\int_0^R \frac{dr}{v_s} \approx 2\int_0^R \frac{dr}{\sqrt{\frac{2}{3}\gamma\pi G\rho\left(R^2 - r^2\right)}},$$

or

$$\boxed{\Pi \approx \sqrt{\frac{3\pi}{2\gamma G\rho}}.} \tag{6}$$

Qualitatively, this shows that the pulsation period of a star is inversely proportional to the square root of its mean density. Referring to Fig. 8 and Table 1, this **period–mean density relation** explains why the pulsation period decreases as we move down the instability strip from the very tenuous supergiants to the very dense white dwarfs.[2] The tight period–luminosity relation discovered by Leavitt exists because the instability strip is roughly parallel to the luminosity axis of the H–R diagram (the finite width of the instability strip is reflected in the ± 0.5 magnitude uncertainty in the period–luminosity relation). The quantitative agreement of Eq. (6) with the observed periods of Cepheids is not too bad, considering its crude derivation. If we take $M = 5\,\mathrm{M}_\odot$ and $R = 50\,\mathrm{R}_\odot$ for a typical Cepheid, then $\Pi \approx 10$ days. This falls nicely within the range of periods measured for the classical Cepheids.

Radial Modes of Pulsation

The sound waves involved in the **radial modes** of stellar pulsation are essentially *standing waves*, similar to the standing waves that occur in an organ pipe that is open at one end; see Fig. 9. Both the star and the organ pipe can sustain several modes of oscillation. The standing wave for each mode has a *node* at one end (the star's center, the pipe's closed end), where the gases do not move, and an *antinode* at the other end (the star's surface, the pipe's open end). For the **fundamental mode**, the gases move in the same direction at every point in the star or pipe. There is a single node between the center and the surface for the **first overtone** mode,[3] with the gases moving in opposite directions on either side of

[2]Pulsating white dwarfs exhibit nonradial oscillations, and their periods are longer than predicted by the period–mean density relation.

[3]Some texts use the unfortunate term *first harmonic* for the first overtone.

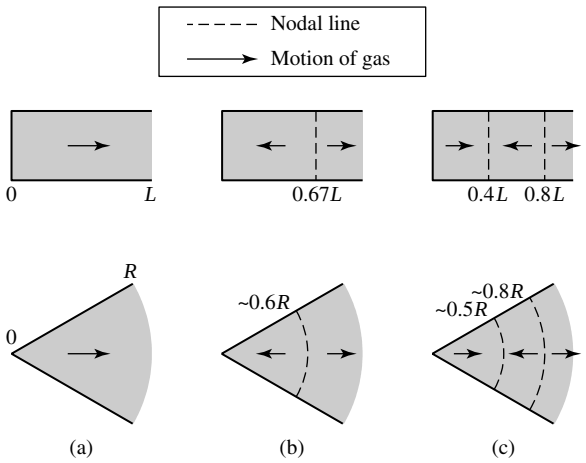

FIGURE 9 Standing sound waves in an organ pipe and in a star for (a) the fundamental mode, (b) the first overtone, and (c) the second overtone.

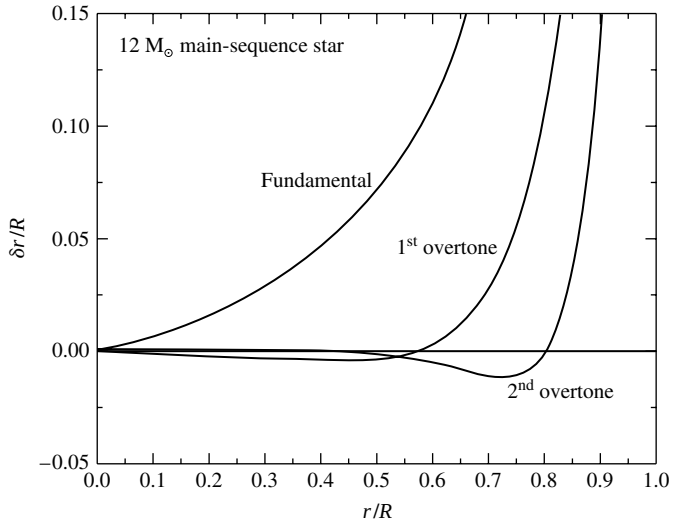

FIGURE 10 Radial modes for a pulsating star. The waveform for each mode has been arbitrarily scaled so that $\delta r/R = 1$ at the surface of the star. Actually, the maximum surface ratio of $\delta r/R$ is approximately 0.05 to 0.10 for a classical Cepheid.

the node, and two nodes for the **second overtone** mode. Figure 10 shows the fractional displacement, $\delta r/R$, of the stellar material from its equilibrium position for several radial modes of a 12 $M_\odot$ main-sequence star model. Note that $\delta r/R$ has been arbitrarily scaled to unity at the stellar surface.

For radial modes, the motion of the stellar material occurs primarily in the surface regions, but there is some oscillation deep inside the star. This effect is most prominent for

the fundamental mode, where non-negligible amplitudes exist. For the stellar model used in Fig. 10, at $r = 0.5R$, $\delta r/R$ is about 7% of its surface value. For the first overtone at the same location, $\delta r/R$ is less than 1% of its surface value and is in the opposite direction, and for the second overtone, the oscillation is nearly zero amplitude ($r = 0.5R$ is close to a node for the second overtone).

The vast majority of the classical Cepheids and W Virginis stars pulsate in the fundamental mode. The RR Lyrae variables pulsate in either the fundamental or the first overtone mode, with a few oscillating in both modes simultaneously. The long-period variables, such as Mira, may also oscillate in either the fundamental mode or the first overtone, although this is still not entirely clear.

Eddington's Thermodynamic Heat Engine

To explain the mechanism that powers these standing sound waves, Eddington proposed that pulsating stars are thermodynamic heat engines. The gases comprising the layers of the star do $P\,dV$ work as they expand and contract throughout the pulsation cycle. If the integral $\oint P\,dV > 0$ for the cycle, a layer does net positive work on its surroundings and contributes to driving the oscillations; if $\oint P\,dV < 0$, the net work done by the layer is negative and tends to dampen the oscillations. Figures 11 and 12 show P–V diagrams for a driving layer and a damping layer, respectively, in a numerical calculation of the oscillation of an RR Lyrae star. If the total work (found by adding up the contributions of all the layers of the star) is positive, the oscillations will grow in amplitude. The oscillations will decay if the total work is negative. These changes in the pulsation amplitude continue until an equilibrium value is reached, when the total work done by all the layers is zero.

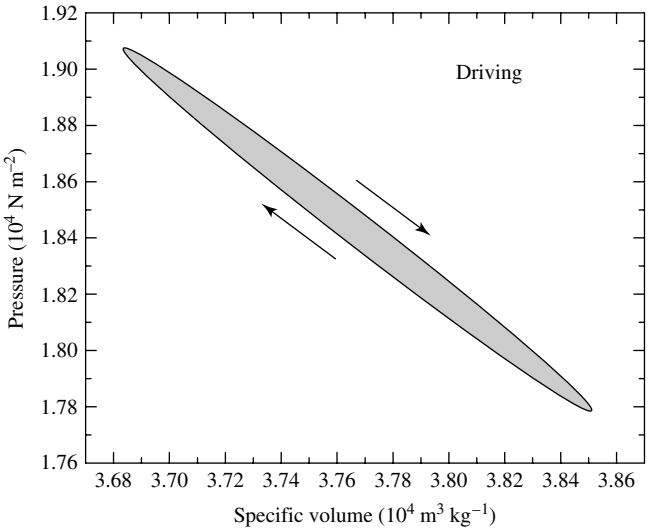

FIGURE 11 P–V diagram for a driving layer of an RR Lyrae star model. You may recall the analogous use of P–V diagrams in discussing heat engines in introductory physics courses. A clockwise path in a P–V diagram corresponds with net driving.

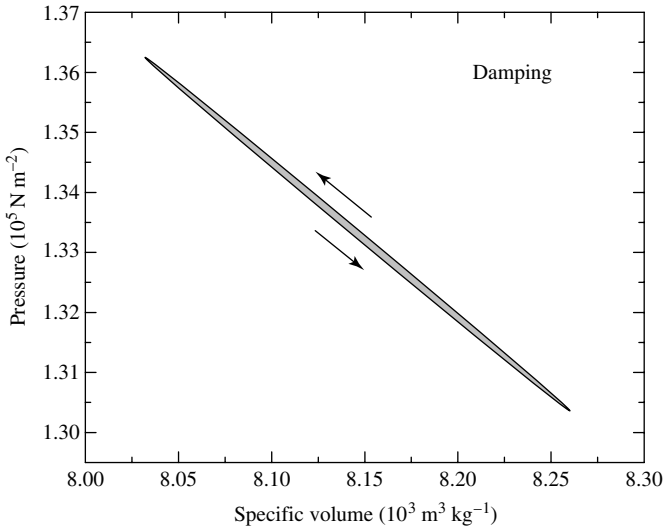

FIGURE 12 P–V diagram for a damping layer of an RR Lyrae star model. A counterclockwise path in a P–V diagram corresponds to net damping.

As for any heat engine, the net work done by each layer of the star during one cycle is the difference between the heat flowing into the gas and the heat leaving the gas. For driving, the heat must enter the layer during the high-temperature part of the cycle and leave during the low-temperature part. Just as the spark plug of an automobile engine fires at the end of the compression stroke, the driving layers of a pulsating star must absorb heat around the time of their maximum compression. In this case the maximum pressure will occur *after* maximum compression, and the oscillations will be amplified.

The Nuclear ϵ Mechanism

In what region of the star can this driving take place? An obvious possibility was first considered by Eddington: When the center of the star is compressed, its temperature and density rise, increasing the rate at which thermonuclear energy is generated. However, recall from Fig. 10 that the displacement $\delta r/R$ has a node at the center of the star. The pulsation amplitude is very small near the center. Although this energy mechanism (called the **ϵ-mechanism**) does in fact operate in the core of a star, it is usually not enough to drive the star's pulsation. However, variations in the nuclear energy generation rate (ϵ) produce oscillations that may contribute to preventing the formation of stars with masses greater than approximately 90 $M_\odot$.

Eddington's Valve

Eddington then suggested an alternative, a *valve mechanism*. If a layer of the star became more opaque upon compression, it could "dam up" the energy flowing toward the surface and push the surface layers upward. Then, as this expanding layer became more transparent, the trapped heat could escape and the layer would fall back down to begin the cycle anew. In Eddington's own words, "To apply this method we must make the star more heat-tight

when compressed than when expanded; in other words, *the opacity must increase with compression*."

In most regions of the star, however, the opacity actually *decreases* with compression. For a Kramers law, the opacity κ depends on the density and temperature of the stellar material as $\kappa \propto \rho/T^{3.5}$. As the layers of a star are compressed, their density and temperature both increase. But because the opacity is more sensitive to the temperature than to the density, the opacity of the gases usually decreases upon compression. It takes special circumstances to overcome the damping effect of most stellar layers, which explains why stellar pulsation is observed for only one of every 10^5 stars.

Opacity Effects and the κ and γ Mechanisms

The conditions responsible for exciting and maintaining the stellar oscillations were first identified by the Russian astronomer S. A. Zhevakin and then verified in detailed calculations by a German and two Americans, Rudolph Kippenhahn, Norman Baker, and John P. Cox (1926–1984). They found that the regions of a star where Eddington's valve mechanism can successfully operate are its *partial ionization zones*. In these layers of the star where the gases are partially ionized, part of the work done on the gases as they are compressed produces further ionization rather than raising the temperature of the gas.[4] With a smaller temperature rise, the increase in density with compression produces a corresponding increase in the Kramers opacity; see Fig. 13. Similarly, during expansion, the temperature does not decrease as much as expected since the ions now recombine with electrons and release energy. Again, the density term in the Kramers law dominates, and

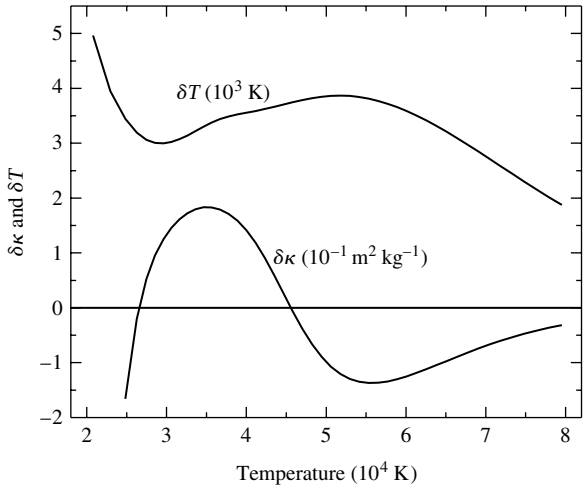

FIGURE 13 Variations in the temperature and opacity throughout an RR Lyrae star model at the time of maximum compression. In the He II partial ionization zone ($T \approx 40{,}000$ K), $\delta\kappa > 0$ and δT is reduced. These are the κ- and γ-mechanisms that drive the star's oscillations.

[4] This causes the specific heats C_P and C_V to have larger values in a partial ionization zone.

the opacity decreases with decreasing density during the expansion. This layer of the star can thus absorb heat during compression, be pushed outward to release the heat during expansion, and fall back down again to begin another cycle. Astronomers refer to this opacity mechanism as the **κ-mechanism**.

In a partial ionization zone, the κ-mechanism is reinforced by the tendency of heat to flow into the zone during compression simply because its temperature has increased less than the adjacent stellar layers. This effect is called the **γ-mechanism**, after the smaller ratio of specific heats caused by the increased values of C_P and C_V. Partial ionization zones are the pistons that drive the oscillations of stars; they modulate the flow of energy through the layers of the star and are the direct cause of stellar pulsation.

The Hydrogen and Helium Partial Ionization Zones

In most stars there are two main ionization zones. The first is a broad zone where both the ionization of neutral hydrogen (H I→H II) and the first ionization of helium (He I→He II) occur in layers with a characteristic temperature of 1 to 1.5 $\times 10^4$ K. These layers are collectively referred to as the **hydrogen partial ionization zone**. The second, deeper zone involves the second ionization of helium (He II→He III), which occurs at a characteristic temperature of 4×10^4 K and is called the **He II partial ionization zone**.

The location of these ionization zones within the star determines its pulsational properties. As shown in Fig. 14, if the star is too hot (7500 K), the ionization zones will be located very near the surface. At this position, the density is quite low, and there is not enough mass available to drive the oscillations effectively. This accounts for the hot **blue edge** of the instability strip on the H–R diagram. In a cooler star (6500 K), the characteristic

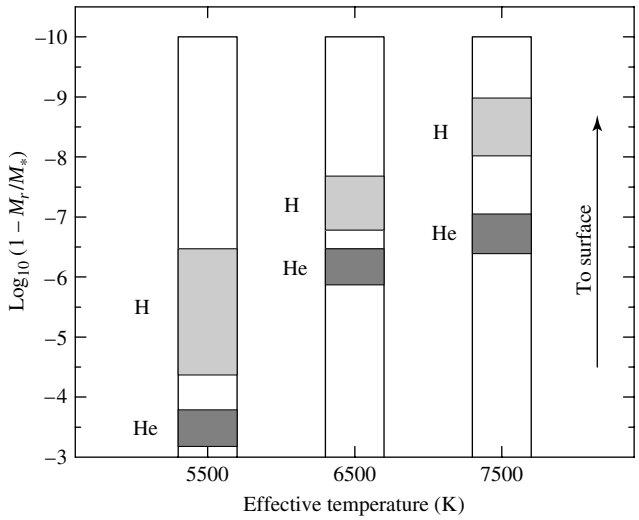

FIGURE 14 Hydrogen and helium ionization zones in stars of different temperatures. For each point in the star, the vertical axis displays the logarithm of the fraction of the star's mass that lies *above* that point.

temperatures of the ionization zones are found deeper in the star. There is more mass for the ionization zone "piston" to push around, and the first overtone mode may be excited. (Whether a mode is actually excited depends on whether the positive work generated within the ionization zones is sufficient to overcome the damping due to negative work of the other layers of the star.) In a still cooler star (5500 K), the ionization zones occur deep enough to drive the fundamental mode of pulsation. However, if a star's surface temperature is too low, the onset of efficient convection in its outer layers may dampen the oscillations. Because the transport of energy by convection is more effective when the star is compressed, the convecting stellar material may lose heat at minimum radius. This could overcome the damming up of heat by the ionization zones—and so quench the pulsation of the star. The cool **red edge** of the instability strip is the result of the damping effect of convection.[5]

Detailed numerical calculations of the pulsation of model stars produce an instability strip that is in good agreement with its observed location on the H–R diagram. These computations show that it is the He II partial ionization zone that is primarily responsible for driving the oscillations of stars within the instability strip. If the effect of the helium ionization zone is artificially removed, the model stars will not pulsate.

The hydrogen ionization zone plays a more subtle role. As a star pulsates, the hydrogen ionization zone moves toward or away from the surface as the zone expands and contracts in response to the changing temperature of the stellar gases. It happens that the star is brightest when the *least mass* lies between the hydrogen ionization zone and the surface. As a star oscillates, the location of an ionization zone changes with respect to both its radial position, r, and its mass interior to r, M_r. The luminosity incident on the *bottom* of the hydrogen ionization zone is indeed a maximum at minimum radius, but this merely propels the zone outward (through mass) most rapidly at that instant. The emergent luminosity is thus greatest *after* minimum radius, when the zone is nearest the surface. This delaying action of the hydrogen partial ionization zone produces the phase lag observed for classical Cepheids and RR Lyrae stars.

The mechanisms responsible for the pulsation of stars outside the instability strip are not always as well understood. The long-period variables are red supergiants (AGB stars) with huge, diffuse convective envelopes surrounding a compact core. Their spectra are dominated by molecular absorption lines and emission lines that reveal the existence of atmospheric shock waves and significant mass loss. While we understand that the *hydrogen* partial ionization zone drives the pulsation of a long-period variable star, many details remain to be explained, such as how its oscillations interact with its outer atmosphere.[6]

β Cephei Stars and the Iron Opacity "Bump"

The β Cephei stars pose another interesting challenge. Being situated in the upper left-hand side of the H–R diagram, these stars are very hot and luminous. β Cepheis are early B stars with effective temperatures in the range of 20,000 to 30,000 K and typically with luminosity classes of III, IV, and V. Given their high effective temperatures, hydrogen is completely

[5]Much work remains to be done on the effect of convection on stellar pulsation, although some results have been obtained for RR Lyrae and ZZ Ceti stars. Progress has been hampered by the present lack of a fundamental theory of time-dependent convection.

[6] The ZZ Ceti stars are also driven by the hydrogen partial ionization zone.

ionized, and the helium ionization zone is too near the surface to effectively drive pulsations in these stars. After years of investigation it was realized that the κ and γ mechanisms are still active in β Cephei stars, but the element responsible for the driving is iron. Although the abundance of iron is low in all stars, the large number of absorption lines in the spectrum of iron implies that iron contributes significantly to stellar opacities at temperatures near 100,000 K. This effect can be seen in the "iron bump" above 100,000 K in the plot of opacity. The depth of this iron ionization region is sufficient to produce net positive pulsational driving in these stars.

3 ■ MODELING STELLAR PULSATION

The star was considered to be divided into a number of concentric mass shells. The differential equations of static stellar structure were then converted into difference equations and applied to each mass shell, and the system of equations was solved on a computer subject to certain boundary conditions at the center and surface of the stellar model.

Nonlinear Hydrodynamic Models

Because a pulsating star is not in hydrostatic equilibrium, the stellar structure equations collected at the beginning of Section 5 cannot be used in their present form. Instead, a more general set of equations is employed that takes the oscillation of the mass shells into account. For example, Newton's second law,

$$\rho \frac{d^2 r}{dt^2} = -G \frac{M_r \rho}{r^2} - \frac{dP}{dr}, \tag{7}$$

must be used for hydrostatic equilibrium. Once the differential equations describing the nonequilibrium mechanical and thermal behavior of a star have been assembled, along with the appropriate constitutive relations, they may be replaced by difference equations and solved numerically. In essence, the model star is mathematically displaced from its equilibrium configuration and then "released" to begin its oscillation. The mass shells expand and contract, pushing against each other as they move. If conditions are right, the ionization zones in the model star will drive the oscillations, and the pulsation amplitude will slowly increase; otherwise the amplitude will decay away. Computer programs that carry out these calculations have been quite successful at modeling the details observed in the light and radial velocity curves of Cepheid variables.

The main advantage of the preceding approach is that it is a **nonlinear** calculation, capable in principle of modeling the complexities of large pulsation amplitudes and reproducing the nonsinusoidal shape of actual light curves. One disadvantage lies in the computer resources required: This process requires a significant amount of CPU time and memory. Many (sometimes thousands of) oscillations must be calculated before the model settles down into a well-behaved periodic motion, and even more periods may be required for the model to reach its *limit cycle*, when the pulsation amplitude has reached its final value. In fact, in some cases the computer simulations of certain classes of pulsating stars may never

attain a truly periodic solution but exhibit chaotic behavior instead, as observed in some real stars.

A second disadvantage of nonlinear calculations lies in the challenges involved in accurately converging models at each time step. Numerical instabilities in the nonlinear equations can cause calculations to misbehave and lead to unphysical solutions. This is particularly true when theories of time-dependent convection are required for red giants and supergiant stars.

Linearizing the Hydrodynamic Equations

An alternative to the nonlinear approach is to **linearize** the differential equations by considering only small-amplitude oscillations. This is done by writing every variable in the differential equations as an equilibrium value (found in the static model of the star) plus a small change due to the pulsation. For example, the pressure P would be written as $P = P_0 + \delta P$, where P_0 is the value of the pressure in a mass shell of the equilibrium model, and δP is the small change in pressure that occurs as that mass shell moves in the oscillating model star. Thus δP is a function of time, but P_0 is constant. When the variables written in this manner are inserted into the differential equations, the terms containing only equilibrium quantities cancel, and terms that involve powers of the deltas higher than the first, such as $(\delta P)^2$, may be discarded because they are negligibly small. The resulting linearized differential equations and their associated boundary conditions, also linearized, are similar to the equations for a wave on a string or in an organ pipe. Only certain standing waves with specific periods are permitted, and so the pulsation modes of the star are cleanly identified. The equations are still sufficiently complicated that a computer solution is required, but the time involved is much less than that required for a nonlinear calculation. The penalties for adopting the linearized approach are that the motion of the star is forced to be sinusoidal (as it must be for small amplitudes of oscillation), and the limiting value of the pulsation amplitude cannot be determined. Modeling the complexities of the full nonlinear behavior of the stellar model is thus sacrificed.

Example 3.1. In this example, we consider an unrealistic, but very instructive, model of a pulsating star called a **one-zone model**; see Fig. 15. It consists of a central point mass equal to the entire mass of the star, M, surrounded by a single thin, spherical shell of mass m and radius R that represents the surface layer of the star. The interior of the shell is filled with a massless gas of pressure P whose sole function is to support the shell against the gravitational pull of the central mass M. Newton's second law (Eq. 7) applied to this shell is

$$m\,\frac{d^2R}{dt^2} = -\frac{GMm}{R^2} + 4\pi R^2 P. \tag{8}$$

For the equilibrium model, the left-hand side of this equation is zero, so

$$\frac{GMm}{R_0^2} = 4\pi R_0^2 P_0. \tag{9}$$

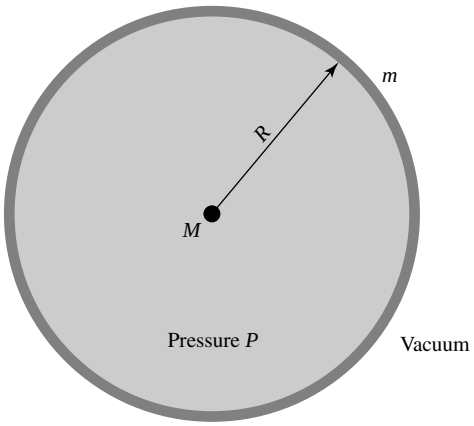

FIGURE 15 One-zone model of a pulsating star.

The linearization is accomplished by writing the star's radius and pressure as

$$R = R_0 + \delta R \qquad \text{and} \qquad P = P_0 + \delta P$$

and inserting these expressions into Eq. (8), giving

$$m\,\frac{d^2(R_0+\delta R)}{dt^2} = -\frac{GMm}{(R_0+\delta R)^2} + 4\pi(R_0+\delta R)^2(P_0+\delta P).$$

Using the first-order approximation

$$\frac{1}{(R_0+\delta R)^2} \approx \frac{1}{R_0^2}\left(1-2\frac{\delta R}{R_0}\right)$$

and keeping only those terms involving the first powers of the deltas results in

$$m\,\frac{d^2(\delta R)}{dt^2} = -\frac{GMm}{R_0^2} + \frac{2GMm}{R_0^3}\,\delta R + 4\pi R_0^2 P_0 + 8\pi R_0 P_0 \delta R + 4\pi R_0^2 \delta P,$$

where $d^2R_0/dt^2 = 0$ has been used for the equilibrium model. The first and third terms on the right-hand side cancel (see Eq. 9), leaving

$$m\,\frac{d^2(\delta R)}{dt^2} = \frac{2GMm}{R_0^3}\,\delta R + 8\pi R_0 P_0 \delta R + 4\pi R_0^2 \delta P. \tag{10}$$

This is the linearized version of Newton's second law for our one-zone model.

To reduce the two variables δR and δP to one, we now assume that the oscillations are *adiabatic*. In this case, the pressure and volume of the model are related by the adiabatic

continued

relation $PV^{\gamma} = \text{constant}$, where γ is the ratio of specific heats of the gas. Since the volume of the one-zone model is just $\frac{4}{3}\pi R^3$, the adiabatic relation says that $PR^{3\gamma} = \text{constant}$. It is left as a problem to show that the linearized version of this expression is

$$\frac{\delta P}{P_0} = -3\gamma \frac{\delta R}{R_0}. \tag{11}$$

Using this equation, δP can be eliminated from Eq. (10). In addition, $8\pi R_0 P_0$ can be replaced by $2GMm/R_0^3$ through the use of Eq. (9). As a result, the mass m of the shell cancels, leaving the linearized equation for δR:

$$\frac{d^2(\delta R)}{dt^2} = -(3\gamma - 4)\frac{GM}{R_0^3}\delta R. \tag{12}$$

If $\gamma > 4/3$ (so the right-hand side of the equation is negative), this is just the familiar equation for simple harmonic motion. It has the solution $\delta R = A\sin(\omega t)$, where A is the pulsation amplitude and ω is the angular pulsation frequency. Inserting this expression for δR into Eq. (12) results in

$$\omega^2 = (3\gamma - 4)\frac{GM}{R_0^3}. \tag{13}$$

Finally, the pulsation period of the one-zone model is just $\Pi = 2\pi/\omega$, or

$$\Pi = \frac{2\pi}{\sqrt{\frac{4}{3}\pi G\rho_0(3\gamma - 4)}}, \tag{14}$$

where $\rho_0 = M/\frac{4}{3}\pi R_0^3$ is the average density of the equilibrium model. For an ideal monatomic gas (appropriate for hot stellar gases), $\gamma = 5/3$. Except for factors of order unity, this is the same as our earlier period estimate (Eq. 6) obtained by considering the time required for a sound wave to cross the diameter of a star.

In Example 3.1, the approximations that the pulsation of the one-zone model was *linear* and *adiabatic* were used to simplify the calculation. Note that the pulsation amplitude, A, canceled in this example. The inability to calculate the amplitude of the oscillations is an inherent drawback of the linearized approach to pulsation.

Nonlinear and Nonadiabatic Calculations

Because no heat is allowed to enter or leave the layers of a stellar model in an adiabatic analysis, the amplitude (whatever it may be) of the oscillation remains constant. However, astronomers need to know which modes will grow and which will decay away. This calculation must include the physics involved in Eddington's valve mechanism. The equations describing the transfer of heat and radiation through the stellar layers must be incorporated in such a *nonadiabatic* computation. These nonadiabatic expressions may also be linearized and solved to obtain the periods and growth rates of the individual modes. However, a more sophisticated and costly *non*linear, *non*adiabatic calculation is needed to reproduce the complicated light and radial velocity

curves that are observed for some variable stars. The computer problem at the end of this chapter asks you to carry out a nonlinear (but still adiabatic) calculation of the pulsation of this one-zone model.

Dynamical Stability

Equation (12) provides a very important insight into the **dynamical stability** of a star. If $\gamma < 4/3$, then the right-hand side of Eq. (12) is positive. The solution is now $\delta R = Ae^{-\kappa t}$, where κ^2 is the same as ω^2 in Eq. (13). Instead of pulsating, the star *collapses* if $\gamma < 4/3$. The increase in gas pressure is not enough to overcome the inward pull of gravity and push the mass shell back out again, resulting in a *dynamically unstable* model.

For the case of *nonadiabatic* oscillations, the time dependence of the pulsation is usually taken to be the real part of $e^{i\sigma t}$, where σ is the complex frequency $\sigma = \omega + i\kappa$. In this expression, ω is the usual pulsation frequency, while κ is a *stability coefficient*. The pulsation amplitude is then proportional to $e^{-\kappa t}$, and $1/\kappa$ is the characteristic time for the growth or decay of the oscillations.

4 ■ NONRADIAL STELLAR PULSATION

As some types of stars pulsate, their surfaces do not move uniformly in and out in a simple "breathing" motion. Instead, such a star executes a more complicated type of **nonradial** motion in which some regions of its surface expand while other areas contract.

Nonradial Oscillations and Spherical Harmonic Functions

Figure 16 shows the angular patterns for several nonradial modes. If the stellar surface is moving outward within the lighter regions, then it is moving inward within the shaded areas. Scalar quantities such as the change in pressure (δP) follow the same pattern, having positive values in some areas and negative values in others. Formally, these patterns are described by the real parts of the spherical harmonic functions, $Y_\ell^m(\theta, \phi)$, where ℓ is a non-negative integer and m is equal to any of the $2\ell + 1$ integers between $-\ell$ and $+\ell$.[7] There are ℓ *nodal circles* (where $\delta r = 0$), with $|m|$ of these circles passing through the poles of the star and the remaining $\ell - |m|$ nodal circles being parallel to the star's equator. If $\ell = m = 0$, then the pulsation is purely radial.

A few examples of $Y_\ell^m(\theta, \phi)$ functions are

$$Y_0^0(\theta, \phi) = K_0^0$$

$$Y_1^0(\theta, \phi) = K_1^0 \cos\theta$$

$$Y_1^{\pm 1}(\theta, \phi) = K_1^{\pm 1} \sin\theta e^{\pm i\phi}$$

[7] Spherical harmonics are often encountered in physics when spherical symmetry is employed. A common example in the undergraduate physics curriculum is the use of spherical harmonics to describe the quantum mechanical wave functions of a hydrogen atom.

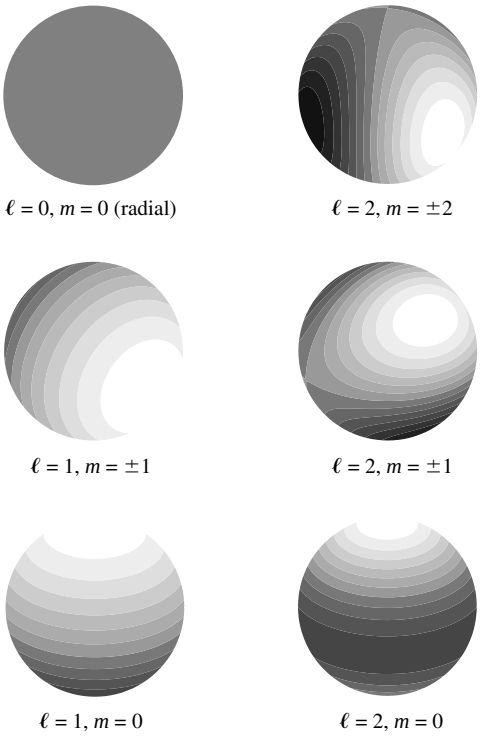

FIGURE 16 Nonradial pulsation patterns. The modes of pulsation are represented by the real parts of the spherical harmonic functions, $Y_\ell^m(\theta, \phi)$.

$$Y_2^0(\theta, \phi) = K_2^0(3\cos^2\theta - 1)$$
$$Y_2^{\pm1}(\theta, \phi) = K_2^{\pm1}\sin\theta\cos\theta e^{\pm i\phi}$$
$$Y_2^{\pm2}(\theta, \phi) = K_2^{\pm2}\cos^2\theta e^{\pm 2i\phi}$$

where the K_ℓ^ms are "normalization" constants and i is the imaginary number $i \equiv \sqrt{-1}$. Recall from Euler's formula that $e^{\pm mi\phi} = \cos(m\phi) \pm i\sin(m\phi)$. Thus, the real part of $e^{\pm mi\phi}$ is just $\cos(m\phi)$.

The patterns for nonzero m represent *traveling waves* that move across the star parallel to its equator. (Imagine these patterns on a beach ball, with the ball slowly spinning about the vertical axis.) The time required for the waves to travel around the star is $|m|$ times the star's pulsation period. However, it is important to note that the star itself may not be rotating at all. Just as water waves may travel across the surface of a lake without the water itself making the trip, these traveling waves are disturbances that pass through the stellar gases.

The p and f Modes

In Section 2, the radial pulsation of stars was attributed to standing sound waves in the stellar interior. For the case of nonradial oscillations, the sound waves can propagate horizontally as well as radially to produce waves that travel around the star. Because *pressure* provides the restoring force for sound waves, these nonradial oscillations are called **p-modes**. A complete description of a p-mode requires specification of its radial and angular nodes. For example, a p_2 mode may be thought of as the nonradial analog of a radial second overtone mode. The p_2 mode with $\ell = 4$ and $m = -3$ has two radial nodes between the center and the surface, and its angular pattern has four nodal lines, three through the poles and one parallel to the equator. Figure 17 shows two p-modes for a 12 $M_\odot$ main-sequence star model; you may note the similarities between this figure and Fig. 10, with most of the motion occurring near the stellar surface. Also shown is the **f-mode**, which can be thought of as a surface gravity wave (note the rapid rise in amplitude with radius). The frequency of the f-mode is intermediate between the p-modes and the g-modes (discussed later). There is no radial analog for the f-mode.

The Acoustic Frequency

An estimate of the angular frequency of a p-mode may be obtained from the time for a sound wave to travel one horizontal wavelength, from one angular nodal line to the next. This horizontal wavelength is given by the expression

$$\lambda_h = \frac{2\pi r}{\sqrt{\ell(\ell+1)}}, \tag{15}$$

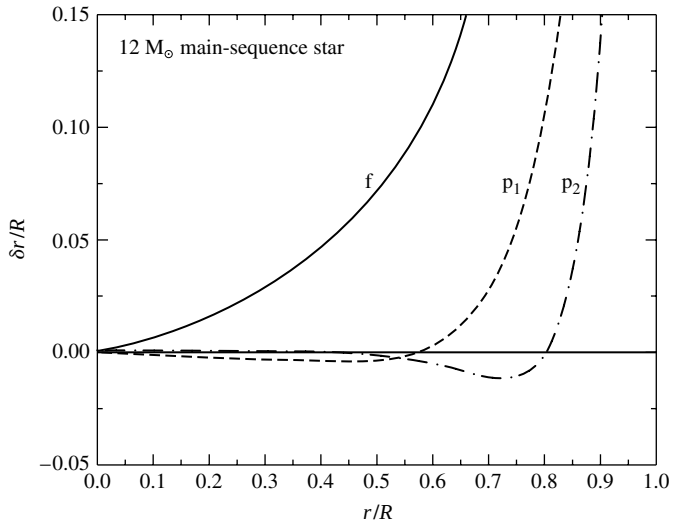

FIGURE 17 Nonradial p-modes with $\ell = 2$. The waveforms have been arbitrarily scaled so that $\delta r/R = 1$ at the star's surface. The f-mode is also shown.

where r is the radial distance from the center of the star. The **acoustic frequency** at this depth in the star is then defined as

$$S_\ell = \frac{2\pi}{\text{time for sound to travel } \lambda_h},$$

which can be written as

$$S_\ell = 2\pi \left[\frac{v_s}{2\pi r/\sqrt{\ell(\ell+1)}} \right] = \sqrt{\frac{\gamma P}{\rho}} \frac{\sqrt{\ell(\ell+1)}}{r}, \tag{16}$$

where v_s is the adiabatic sound speed. Because the speed of sound is proportional to the square root of the temperature [recall from the ideal gas law, that $P/\rho \propto T$], the acoustic frequency is large in the deep interior of the star and decreases with increasing r. The frequency of a p-mode is determined by the average value of S_ℓ, with the largest contributions to the average coming from the regions of the star where the oscillations are most energetic.

In the absence of rotation, the pulsation period depends only on the number of radial nodes and the integer ℓ. The period is independent of m because with no rotation there are no well-defined poles or equator; thus m has no physical significance. On the other hand, if the star is rotating, the rotation itself defines the poles and equator, and the pulsation frequencies for modes with different values of m become separated or *split* as the traveling waves move either with or against the rotation (the sign of m determines the direction in which the waves move around the star). The amount by which the pulsation frequencies are split depends on the angular rotation frequency, Ω, of the star, with the rotationally produced shift in frequency proportional to the product $m\Omega$ for the simple case of uniform rotation. As we will discuss later, this frequency splitting provides a powerful probe for measuring the rotation of the Sun's interior.

The g Modes

Just as pressure supplies the restoring force for the compression and expansion of the p-mode sound waves, *gravity* is the source of the restoring force for another class of nonradial oscillations called **g-modes**. The g-modes are produced by *internal gravity waves*. These waves involve a "sloshing" back and forth of the stellar gases, which is ultimately connected to the *buoyancy* of stellar material. Because "sloshing" cannot occur for purely radial motion, there are no radial analogs for the g-modes.

The Brunt–Väisälä (Buoyancy) Frequency

To gain a better understanding of this oscillatory motion for g-modes, consider a small bubble of stellar material that is displaced upward from its equilibrium position in the star

by an amount dr.[8] We will assume that this motion occurs

1. slowly enough that the pressure within the bubble, $P^{(b)}$, is always equal to the pressure of its surroundings, $P^{(s)}$; and
2. rapidly enough that there is no heat exchanged between the bubble and its surroundings.

The second assumption means that the expansion and compression of the gas bubble are *adiabatic*. If the density of the displaced bubble is greater than the density of its new surroundings, the bubble will fall back to its original position. The net restoring force *per unit volume* on the bubble in its final position is the difference between the upward buoyant force (given by Archimedes's law) and the downward gravitational force:

$$f_{\text{net}} = \left(\rho_f^{(s)} - \rho_f^{(b)}\right) g,$$

where $g = GM_r/r^2$ is the local value of the gravitational acceleration. Using a Taylor expansion for the densities about their initial positions results in

$$f_{\text{net}} = \left[\left(\rho_i^{(s)} + \frac{d\rho^{(s)}}{dr}\,dr\right) - \left(\rho_i^{(b)} + \frac{d\rho^{(b)}}{dr}\,dr\right)\right] g.$$

The initial densities of the bubble and its surroundings are the same, so these terms cancel, leaving

$$f_{\text{net}} = \left(\frac{d\rho^{(s)}}{dr} - \frac{d\rho^{(b)}}{dr}\right) g\,dr.$$

Because the motion of the bubble is adiabatic, $d\rho^{(b)}/dr$ can be replaced:

$$f_{\text{net}} = \left(\frac{d\rho^{(s)}}{dr} - \frac{\rho_i^{(b)}}{\gamma P_i^{(b)}}\frac{dP^{(b)}}{dr}\right) g\,dr.$$

Looking at this equation, all of the "b" superscripts may be changed to "s" because the initial densities are equal, and according to the first assumption given, the pressures inside and outside the bubble are *always* the same. Thus all quantities in this equation refer to the stellar material surrounding the bubble. With that understanding, the subscripts may be dropped completely, resulting in

$$f_{\text{net}} = \left(\frac{1}{\rho}\frac{d\rho}{dr} - \frac{1}{\gamma P}\frac{dP}{dr}\right) \rho g\,dr.$$

For convenience, the term in parentheses is defined as

$$A \equiv \frac{1}{\rho}\frac{d\rho}{dr} - \frac{1}{\gamma P}\frac{dP}{dr}. \tag{17}$$

[8] The following discussion is just a reexamination of the problem of convection from another perspective.

Thus the net force per unit volume acting on the bubble is

$$f_{\text{net}} = \rho A g \, dr. \tag{18}$$

If $A > 0$, the net force on the displaced bubble has the same sign as dr, and so the bubble will continue to move away from its equilibrium position. This is the condition necessary for *convection* to occur, and it is equivalent to the other requirements previously found for convective instability. However, if $A < 0$, then the net force on the bubble will be in a direction opposite to the displacement, and so the bubble will be pushed back toward its equilibrium position. In this case, Eq. (18) has the form of Hooke's law, with the restoring force proportional to the displacement. Thus if $A < 0$, the bubble will oscillate about its equilibrium position with simple harmonic motion.

Dividing the force per unit volume, f_{net}, by the mass per unit volume, ρ, gives the force per unit mass, or acceleration: $a = f_{\text{net}}/\rho = A g \, dr$. Because the acceleration is simply related to the displacement for simple harmonic motion,[9] we have

$$a = -N^2 \, dr = A g \, dr,$$

where N is the angular frequency of the bubble about its equilibrium position, called the **Brunt–Väisälä frequency** or the **buoyancy frequency**,

$$\boxed{N = \sqrt{-Ag} = \sqrt{\left(\frac{1}{\gamma P} \frac{dP}{dr} - \frac{1}{\rho} \frac{d\rho}{dr} \right) g}.} \tag{19}$$

The buoyancy frequency is zero at the center of the star (where $g = 0$) and at the edges of convection zones (where $A = 0$). Recall that $A < 0$ where there is no convection, so N is larger in regions that are more stable against convection. Inside a convection zone, where $A > 0$, the buoyancy frequency is not defined.

The g and p Modes as Probes of Stellar Structure

The "sloshing" effect of neighboring regions of the star produces the internal gravity waves that are responsible for the g-modes of a nonradially pulsating star. The frequency of a g-mode is determined by the value of N averaged across the star. Figure 18 shows several g-modes for the same stellar model that was used for Fig. 17. A comparison of these two figures reveals significant differences between these classes of modes, making them very useful to astronomers attempting to study the interior of the Sun and other stars. Most important, notice the difference in the vertical scales of the two figures. The g-modes involve significant movement of the stellar material deep within the star, while the p-mode's motions are confined near the stellar surface. Thus g-modes provide a view into the very heart of a star, while p-modes allow a diagnosis of the conditions in its surface layers.

[9] For example, recall that $F = ma = -kx$ for a spring. The acceleration is $a = -\omega^2 x$, where $\omega = \sqrt{k/m}$ is the angular frequency of the spring's motion.

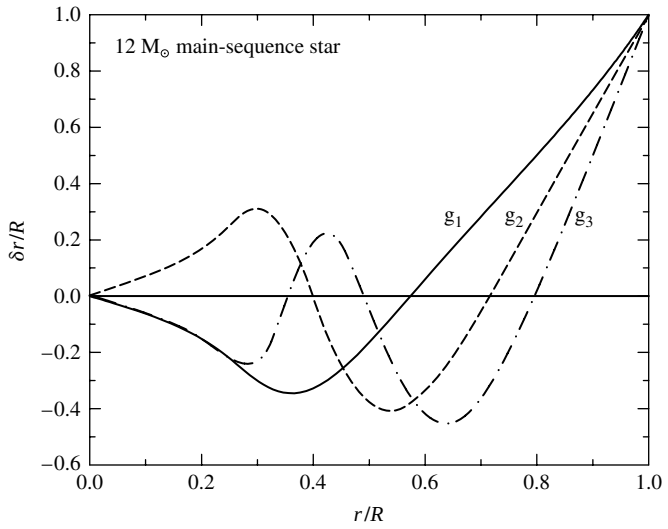

FIGURE 18 Nonradial g-modes with $\ell = 2$. The waveforms have been arbitrarily scaled so that $\delta r/R = 1$ at the star's surface.

5 ■ HELIOSEISMOLOGY AND ASTEROSEISMOLOGY

All of the ideas of nonradial pulsation come into play in the science of **helioseismology**, the study of the oscillations of the Sun first observed in 1962 by American astronomers Robert Leighton (1919–1997), Robert Noyes, and George Simon. A typical solar oscillation mode has a very low amplitude, with a surface velocity of only 0.10 m s^{-1} or less,[10] and a luminosity variation $\delta L/L_\odot$ of only 10^{-6}. With an incoherent superposition of roughly *ten million* modes rippling through its surface and interior, our star is "ringing" like a bell.

The Five-Minute Solar Oscillations

The oscillations observed on the Sun have modes with periods between three and eight minutes and very short horizontal wavelengths (ℓ ranging from 0 to 1000 or more). These so-called *five-minute oscillations* have been identified as p-modes. The five-minute p-modes are concentrated below the photosphere within the Sun's convection zone; Fig. 19 shows a typical p-mode. g-modes are located deep in the solar interior, below the convection zone. By studying these p-mode oscillations, astronomers have been able to gain new insights into the structure of the Sun in these regions.[11]

[10]These incredibly precise velocity measurements are made by carefully observing the Doppler shifts of spectral absorption lines such as Fe I (557.6099 nm) through a narrow slit that follows the rotating solar surface.

[11]A series of 160-minute "g-modes" were believed to have been observed as well. However, continuous observations over 690 days using the GOLF instrument onboard the SOHO spacecraft were unable to detect any evidence of the controversial mode. It is believed that ground-based observations that indicated a 160-minute mode were due to harmonic effects associated with Earth's atmosphere; note that 160 minutes is exactly 1/9 of the 24-hour solar day.

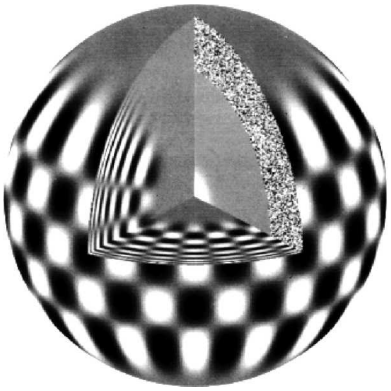

FIGURE 19 Five-minute p_{15} mode with $\ell = 20$ and $m = 16$. The solar convection zone is the stippled region, where the p-modes are found. (Courtesy of National Optical Astronomy Observatories.)

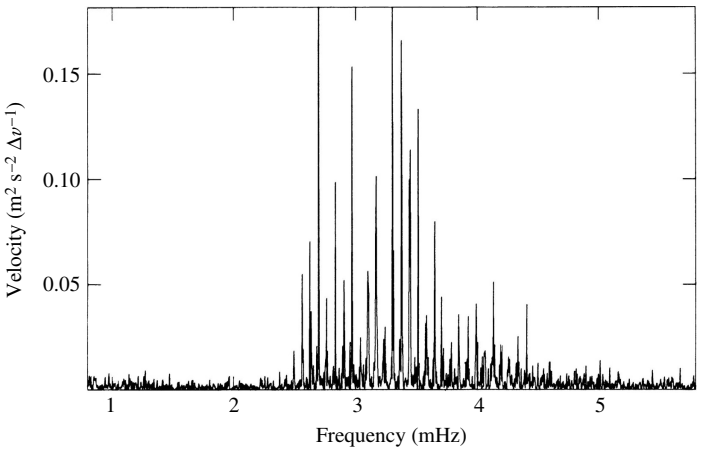

FIGURE 20 Relative power of solar p-modes; a period of five minutes corresponds to a frequency of 3.33 mHz. (Figure adapted from Grec, Fossat, and Pomerantz, *Nature*, *288*, 541, 1980.)

Figure 20 shows the relative power contained in the solar p-modes. This information can also be plotted in another manner, as shown in Fig. 21, with ℓ on the horizontal axis and the pulsation frequency on the vertical axis. Circles show the observed frequencies, and each continuous ridge corresponds to a different p-mode (p_1, p_2, p_3, etc.). The superimposed lines are the *theoretical* frequencies calculated for a solar model. All of the observed five-minute modes have been identified in this way. The fit is certainly impressive but not quite exact. A solar model must be carefully tuned to obtain the best agreement between the theoretical and observed p-mode frequencies. This procedure can reveal much about the depth of the solar convection zone and about the rotation and composition of the outer layers of the Sun.

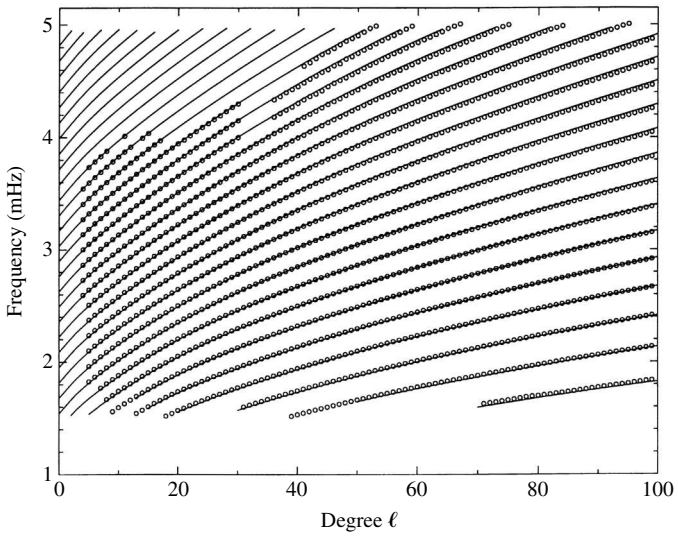

FIGURE 21 Solar p-modes: observations (circles) and theory (lines). (Figure adapted from Libbrecht, *Space Sci. Rev.*, *47*, 275, 1988.)

Differential Rotation and the Solar Convection Zone

Based on helioseismology studies, combined with detailed stellar evolution calculations, the base of the solar convection zone is known to be located at 0.714 $R_\odot$, with a temperature of about 2.18×10^6 K. The rotational splitting observed for p-mode frequencies indicates that differential rotation observed at the Sun's surface decreases slightly down through the convection zone. Those p-modes with shorter horizontal wavelengths (larger ℓ) penetrate less deeply into the convection zone, so the difference in rotational frequency splitting with ℓ reveals the depth dependence of the rotation. The measurement of the variation in rotation with the distance from the solar equator comes from the dependence of the rotational frequency splitting on m. Below the convection zone, the equatorial and polar rotation rates converge to a single value at $r/R_\odot \approx 0.65$. Because a change in the rotation rate with depth is needed to convert the Sun's magnetic field from a poloidal to a toroidal geometry, these results indicate that the Sun's magnetic dynamo is probably seated in the tachocline at the interface between the radiation zone and the convection zone.

Tests of Composition

The abundance of helium in the outer layers of the Sun can also be inferred from a comparison of the observed and theoretical p-mode ridges in Fig. 21. The results are consistent with a value of $Y = 0.2437$ for the mass fraction of helium at the Sun's surface.

Probing the Deep Interior

Astronomers have experienced more difficulty in their attempts to use the solar g-modes as a probe of the Sun's interior. Because the g-modes dwell beneath the convection zone,

their amplitudes are significantly diminished at the Sun's surface. To date, no definite identification of g-modes has been made. Nevertheless, the potential rewards of using these oscillations to learn more about the core of the Sun compel astronomers to apply their observational ingenuity to these g-modes.

Driving Solar Oscillations

The question of the mechanism responsible for driving the solar oscillations has not yet been conclusively answered. Our main-sequence Sun is not a normal pulsating star. It lies far beyond the red edge of the instability strip on the H–R diagram (see Fig. 8) where turbulent convection overcomes the tendency of the ionization zones to absorb heat at maximum compression. Eddington's valve mechanism thus cannot be responsible for the solar oscillations. However, the timescale for convection near the top of the convection zone is a few minutes, and it is strongly suspected that the p-modes are driven by tapping into the turbulent energy of the convection zone itself, where the p-modes are confined.

δ Scuti Stars and Rapidly Oscillating Ap Stars

The techniques of helioseismology can be applied to other stars as well. **Asteroseismology** is the study of the pulsation modes of stars in order to investigate their internal structures, chemical composition, rotation, and magnetic fields.

δ Scuti stars are Population I main-sequence stars and giant stars in the spectral class range A to F. They tend to pulsate in low-overtone radial modes, as well as in low-order p-modes (and possibly g-modes). The amplitudes of δ Scutis are fairly small, ranging from a few mmag to roughly 0.8 mag. Population II subgiants also exhibit radial and nonradial oscillations and are known as SX Phoenicis stars.

Another interesting class of pulsating stars are the **rapidly oscillating Ap stars** (roAp), found in the same portion of the H–R diagram as the δ Scuti stars. These stars have peculiar surface chemical compositions (hence the "p" designation), are rotating, and have strong magnetic fields. The unusual chemical composition is likely due to settling of heavier elements, similar to the elemental diffusion that has occurred near the surface of the Sun. Some elements may also have been elevated in the atmosphere if they have a significant number of absorption lines near the peak of the star's blackbody spectrum. These atoms preferentially absorb photons that impart a net upward momentum. If the atmosphere is sufficiently stable against turbulent motions, some of these atoms will tend to drift upward.

roAp stars have very small pulsation amplitudes of less than 0.016 mag. It appears that they primarily pulsate in higher-order p-modes and that the axis for the pulsation is aligned with the magnetic field axis, which is tilted somewhat to the rotation axis (an oblique rotator model). roAp stars are among the most well-studied of main-sequence stars other than the Sun, but the pulsation driving mechanism still remains in question.

SUGGESTED READING

General

The American Association of Variable Star Observers, `http://www.aavso.org/`.
Giovanelli, Ronald, *Secrets of the Sun*, Cambridge University Press, Cambridge, 1984.

Kaler, James B., *Stars and Their Spectra*, Cambridge University Press, Cambridge, 1997.

Leibacher, John W., et al., "Helioseismology," *Scientific American*, September 1985.

Zirker, Jack B., *Sunquakes: Probing the Interior of the Sun*, Johns Hopkins University Press, Baltimore, 2003.

Technical

Aller, Lawrence H., *Atoms, Stars, and Nebulae*, Third Edition, Cambridge University Press, Cambridge, 1991.

Brown, Timothy M., et al., "Inferring the Sun's Internal Angular Velocity from Observed p-Mode Frequency Splittings," *The Astrophysical Journal*, *343*, 526, 1989.

Clayton, Donald D., *Principles of Stellar Evolution and Nucleosynthesis*, University of Chicago Press, Chicago, 1983.

Cox, John P., *The Theory of Stellar Pulsation*, Princeton University Press, Princeton, NJ, 1980.

Freedman, Wendy L., et al., "Distance to the Virgo Cluster Galaxy M100 from Hubble Space Telescope Observations of Cepheids," *Nature*, *371*, 757, 1994.

General Catalogue of Variable Stars, Sternberg Astronomical Institute, Moscow, Russia, `http://www.sai.msu.su/groups/cluster/gcvs/gcvs/`.

Hansen, Carl J., Kawaler, Steven D., and Trimble, Virginia *Stellar Interiors: Physical Principles, Structure, and Evolution*, Second Edition, Springer-Verlag, New York, 2004.

Perrson, S. E., et al., "New Cepheid Period–Luminosity Relations for the Large Magellanic Cloud: 92 Near-Infrared Light Curves," *The Astronomical Journal*, *128*, 2239, 2004.

Svestka, Zdenek, and Harvey, John W. (eds.), *Helioseismic Diagnostics of Solar Convection and Activity*, Kluwer Academic Publishers, Dordrecht, 2000.

Stellar Pulsation

PROBLEM SET

1 Use the light curve for Mira, Fig. 1, to estimate the ratio of Mira's luminosity at visible wavelengths, when it is brightest to when it is dimmest. For what fraction of its pulsation cycle is Mira visible to the naked eye?

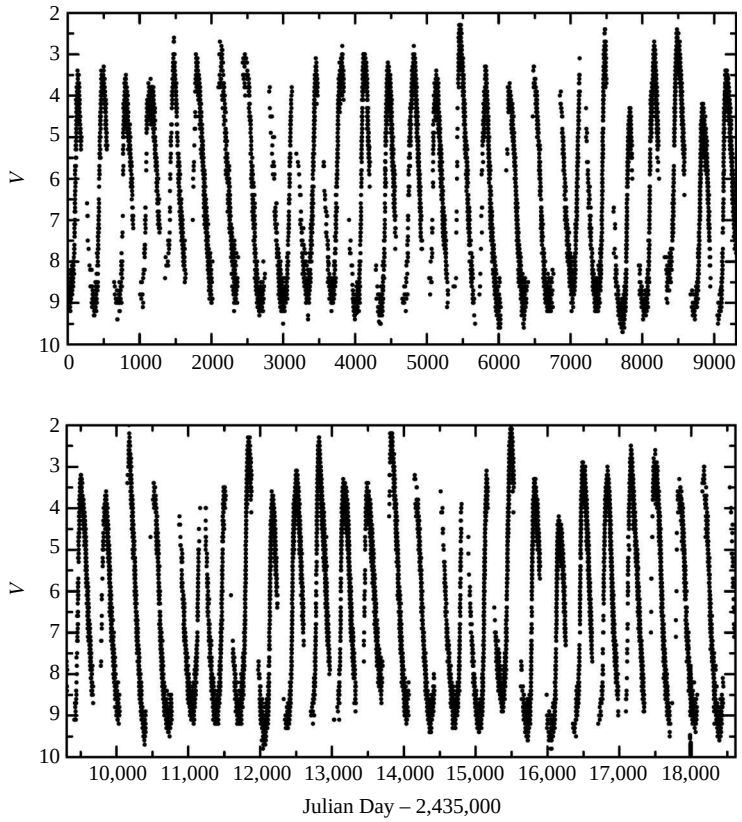

FIGURE 1 The light curve of Mira from September 14, 1954 (JD 2,435,000) through September 2005. Recall that magnitudes dimmer than 6 are undetectable to the unaided eye. (We acknowledge with thanks the variable-star observations from the AAVSO International Database contributed by observers worldwide.)

2 If the intrinsic uncertainty in the period–luminosity relation shown in Fig. 5 is $\Delta M \approx 0.5$ magnitude, find the resulting fractional uncertainty in the calculated distance to a classical Cepheid.

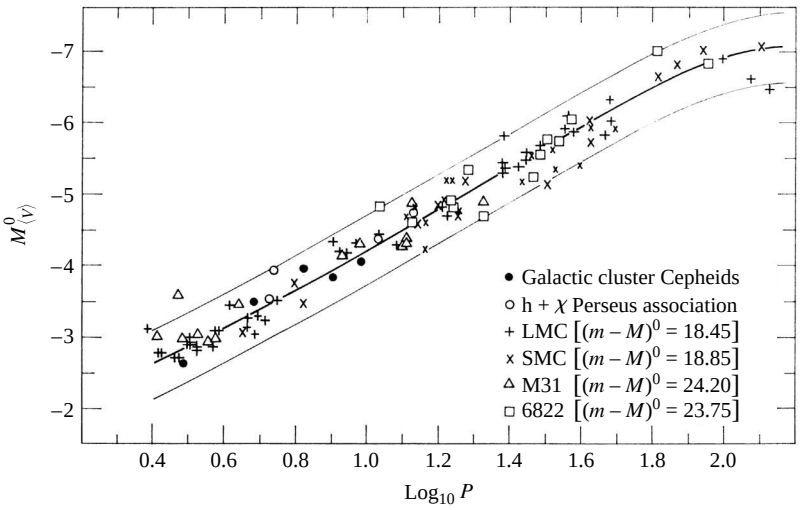

FIGURE 5 The period–luminosity relation for classical Cepheids. (Figure adapted from Sandage and Tammann, *Ap. J., 151*, 531, 1968.)

3 Several remote classical Cepheids were discovered in 1994 by the Hubble Space Telescope in the galaxy denoted M100. (M100 is a member of the Virgo cluster, a rich cluster of galaxies.) Figure 22 shows the period–luminosity relation for these Cepheids. Use the two Cepheids nearest the figure's best-fit line to estimate the distance to M100. The mean visual extinction is $A_V = 0.15 \pm 0.17$ magnitudes for the M100 Cepheids. Compare your result to the distance of 17.1 ± 1.8 Mpc obtained by Wendy Freedman and her colleagues. You are referred to Freedman et al. (1994) for more information on the discovery and importance of these remote pulsating stars.

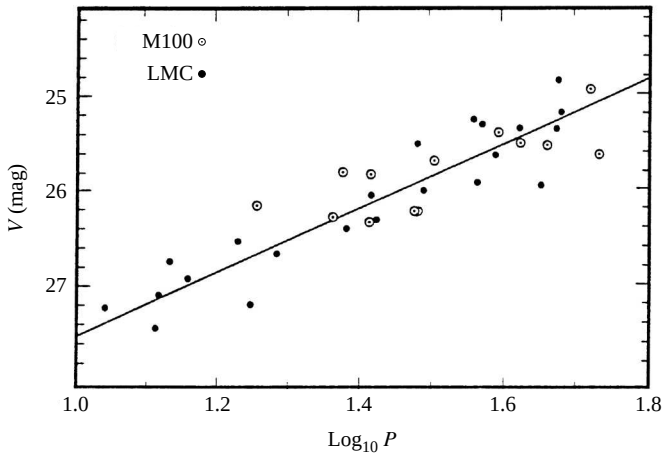

FIGURE 22 A composite period–luminosity relation for Problem 3. The white circles denote Cepheids in M100, and the black circles show nearby Cepheids found in the Large Magellanic Cloud (a small galaxy that neighbors our Milky Way Galaxy). The average visual magnitudes of the LMC Cepheids have been increased by the same amount to match those of the M100 variables. The required increase in V for a best fit is then used to find the relative distances to the LMC and M100. (Adapted from Freedman et al., *Nature, 371*, 757, 1994.)

4 Make a graph similar to Fig. 5 showing the period–luminosity relation for both the classical Cepheids and W Virginis stars.

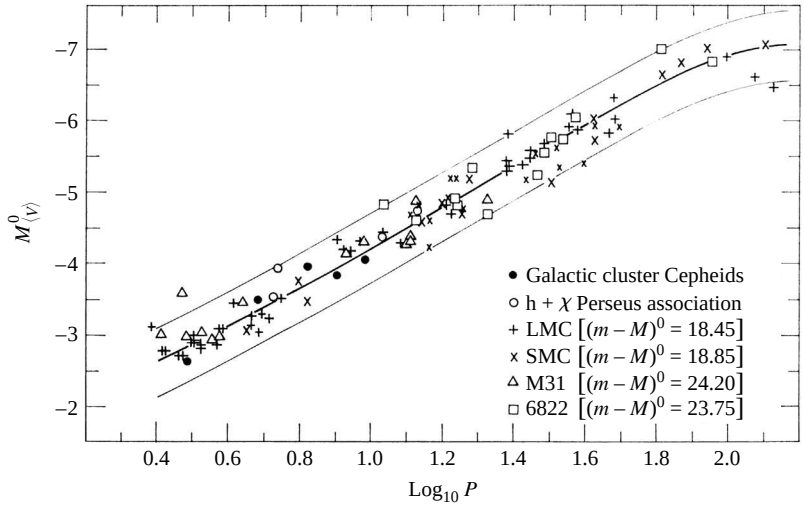

FIGURE 5 The period–luminosity relation for classical Cepheids. (Figure adapted from Sandage and Tammann, *Ap. J., 151*, 531, 1968.)

5 Assuming (incorrectly) that the oscillations of δ Cephei are sinusoidal, calculate the greatest excursion of its surface from its equilibrium position.

6 Use Eq. (6) to estimate the pulsation period that the Sun would have if it were to oscillate radially.

$$\boxed{\Pi \approx \sqrt{\frac{3\pi}{2\gamma G\rho}}.} \tag{6}$$

7 Derive Eq. (11) by linearizing the adiabatic relation

$$PV^\gamma = \text{ constant.}$$

$$\frac{\delta P}{P_0} = -3\gamma\,\frac{\delta R}{R_0}. \tag{11}$$

8 **(a)** Linearize the Stefan–Boltzmann equation in the form of the below equation to show that

$$\frac{\delta L}{L_0} = 2\,\frac{\delta R}{R_0} + 4\,\frac{\delta T}{T_0}.$$

$$\boxed{L = 4\pi R^2 \sigma T_e^4.}$$

(b) Linearize the adiabatic relation $TV^{\gamma-1} =$ constant, and so find a relation between $\delta L/L_0$ and $\delta R/R_0$ for a spherical blackbody model star composed of an ideal monatomic gas.

9 Consider a general potential energy function, $U(r)$, for a force $\mathbf{F} = -(dU/dr)\hat{\mathbf{r}}$ on a particle of mass m. Assume that the origin ($r = 0$) is a point of stable equilibrium. By expanding $U(r)$ in a Taylor series about the origin, show that if a particle is displaced slightly from the origin and then released, it will undergo simple harmonic motion about the origin. This explains why the linearization procedure of Section 3 of "Stellar Pulsation" is guaranteed to result in sinusoidal oscillations.

10 Figure 23 shows a view of a hypothetical nonradially pulsating ($\ell = 2, m = -2$), rotating star from above the star's north pole. From the vantage point of Earth, astronomers view the star along its equatorial plane. Assuming that a spectral absorption line appears when the bottom of Fig. 23 is facing Earth, sketch the changes in the appearance of the line profile due to Doppler shifts caused by the total surface velocity as the star rotates. (Don't worry about the timing; just sketch the spectral line as seen from the eight different points of view shown that are directly over the star's equator.) Assume that the equivalent width of the line does not change. You may wish to compare your line profiles with those actually observed for a nonradially pulsating star such as the β Cephei star 12 Lacertae; see Smith, *Ap. J.*, *240*, 149, 1980. For convenience, the magnitudes of the rotation and pulsation velocities are assumed to be equal.

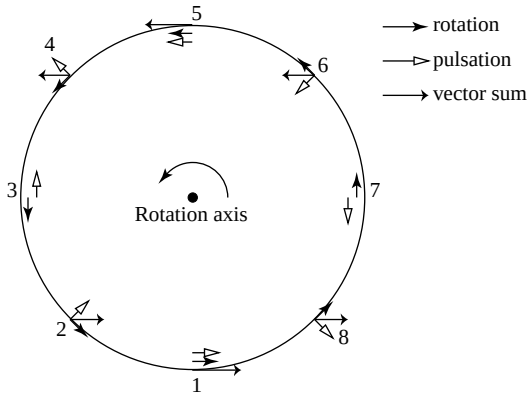

FIGURE 23 Surface velocities for a rotating, pulsating star ($\ell = 2, m = -2$) for Problem 10. The arrows indicate the surface velocities due to rotation alone, pulsation alone, and their vector sum.

11 Show that the below equation, the condition for convection to occur, is the same as the requirement that $A > 0$, where A is given by Eq. (17). Assume that the mean molecular weight, μ, does not vary.

$$\left|\frac{dT}{dr}\right|_{\text{act}} > \left|\frac{dT}{dr}\right|_{\text{ad}}.$$

$$A \equiv \frac{1}{\rho}\frac{d\rho}{dr} - \frac{1}{\gamma P}\frac{dP}{dr}. \tag{17}$$

12 In a convection zone, the timescale for convection is related to the value of A (Eq. 17) by

$$t_c \simeq 2\sqrt{2/Ag}.$$

$$A \equiv \frac{1}{\rho}\frac{d\rho}{dr} - \frac{1}{\gamma P}\frac{dP}{dr}. \tag{17}$$

Table 2 shows the values of the pressure and density at two points near the top of the Sun's convection zone as described by a solar model. Use these values and $\gamma = 5/3$ to obtain an estimate of the timescale for convection near the top of the Sun's convection zone. How does your answer compare with the range of periods observed for the Sun's p-modes?

TABLE 2 Data from a Solar Model for Problem 12. (Data from Joyce Guzik, private communication.)

r (m)	P (N m^{-2})	ρ (kg m^{-3})
6.959318×10^8	9286.0	2.2291×10^{-4}
6.959366×10^8	8995.7	2.1925×10^{-4}

COMPUTER PROBLEM

13 In this problem you will carry out a nonlinear calculation of the radial pulsation of the one-zone model described in Example 3.1 of "Stellar Pulsation." The equations that describe the oscillation of this model star are Newton's second law for the forces on the shell,

$$m\frac{dv}{dt} = -\frac{GMm}{R^2} + 4\pi R^2 P, \tag{20}$$

and the definition of the velocity, v, of the mass shell,

$$v = \frac{dR}{dt}. \tag{21}$$

As in Example 3.1, we assume that the expansion and contraction of the gas are adiabatic:

$$P_i V_i^{\gamma} = P_f V_f^{\gamma}, \tag{22}$$

where the "initial" and "final" subscripts refer to any two instants during the pulsation cycle.

(a) Explain in words the meaning of each term in Eq. (20).

$$m\frac{dv}{dt} = -\frac{GMm}{R^2} + 4\pi R^2 P, \tag{20}$$

(b) Use Eq. (22) to show that

$$P_i R_i^{3\gamma} = P_f R_f^{3\gamma}. \tag{23}$$

(c) You will not be taking derivatives. Instead, you will take the difference between the initial and final values of the radius R and radial velocity v of the shell divided by the time interval Δt separating the initial and final values. That is, you will use $(v_f - v_i)/\Delta t$ instead of dv/dt, and $(R_f - R_i)/\Delta t$ instead of dR/dt in Eqs. (20) and (21). A careful analysis shows that you should use $R = R_i$ and $P = P_i$ on the right-hand side of Eq. (20), and use $v = v_f$ on the left-hand side of Eq. (21). Make these substitutions in Eqs. (20) and (21), and show that you can write

$$m\frac{dv}{dt} = -\frac{GMm}{R^2} + 4\pi R^2 P, \tag{20}$$

$$v = \frac{dR}{dt}. \tag{21}$$

$$v_f = v_i + \left(\frac{4\pi R_i^2 P_i}{m} - \frac{GM}{R_i^2}\right)\Delta t \tag{24}$$

and

$$R_f = R_i + v_f \Delta t. \tag{25}$$

(d) Now you are ready to calculate the oscillation of the model star. The mass of a typical classical Cepheid is $M = 1 \times 10^{31}$ kg (5 $M_\odot$), and the mass of the surface layers may be arbitrarily assigned $m = 1 \times 10^{26}$ kg. For starting values at time $t = 0$, take

$$R_i = 1.7 \times 10^{10} \text{ m}$$

$$v_i = 0 \text{ m s}^{-1}$$

$$P_i = 5.6 \times 10^4 \text{ N m}^{-2}$$

and use a time interval of $\Delta t = 10^4$ s. Take the ratio of specific heats to be $\gamma = 5/3$ for an ideal monatomic gas. Use Eq. (24) to calculate the final velocity v_f at the end of one time interval (at time $t = 1 \times 10^4$ s); then use Eq. (25) to calculate the final radius R_f and Eq. (23) to calculate the final pressure P_f. Now take these final values to be your new initial values, and find new values for R, v, and P after two time intervals (at time $t = 2 \times 10^4$ s). Continue to find R, v, and P for 150 time intervals, until $t = 1.5 \times 10^6$ s. Make three graphs of your results: R vs. t, v vs. t, and P vs. t. Plot the time on the horizontal axis.

$$v_f = v_i + \left(\frac{4\pi R_i^2 P_i}{m} - \frac{GM}{R_i^2} \right) \Delta t \tag{24}$$

$$R_f = R_i + v_f \Delta t. \tag{25}$$

(e) From your graphs, measure the period Π of the oscillation (both in seconds and in days) and the equilibrium radius, R_0, of the model star. Compare this value of the period with that obtained from Eq. (14). Also compare your results with the period and radial velocity observed for δ Cephei.

$$\Pi = \frac{2\pi}{\sqrt{\frac{4}{3}\pi G \rho_0 (3\gamma - 4)}}, \tag{14}$$